The International Journal of Engineering and Science (IJES)
|| Volume || 13 || Issue || 4 || Pages || PP 98-110 || 2024 ||
ISSN (e): 2319 – 1813 ISSN (p): 2319 – 1805

Erosion Patterns Analysis of GQX172 Core Extraction Tool's Diverter Shaft

Xiangyu Z[1], Liping T[1]

[1]*School of Mechatronic Engineering, Southwest Petroleum University, Chengdu, China*

Corresponding Author: Liping T

----------*ABSTRACT*----------

With the development of drilling exploration towards deep and ultra-deep wells, conventional core drilling tools cannot meet the core drilling requirements under complex geological conditions. Therefore, a high-strength GQX type slim hole coring tool has been designed and developed. In this study, the failure problem of the outer tube and flow channel holes of the core drilling tool due to erosion and wear during use was investigated. The erosion law of the diverter shaft was studied by using the Discrete Phase Model (DPM) in computational fluid dynamics software. The results show that the drilling fluid flow rate and particle mass flow rate are basically linearly related to the erosion rate. The maximum erosion rate and average erosion rate under different particle diameters are both increasing first and then decreasing. The tilt angle of the diverter holes controlled within the range of 40°~50° can effectively reduce the erosion rate. The increase in the width of the diverter holes will quickly reduce the erosion rate. After reaching a certain range, the erosion rate will gradually stabilize. The length of the diverter holes has a small effect on the erosion rate, so its strength requirements should be met.

KEYWORDS;- *Coring tool; Liquid-solid; Erosion rate; Numerical simulation*

Date of Submission: 05-04-2024 Date of acceptance: 17-04-2024

I. INTRODUCTION

The traditional way of oil and gas extraction is mainly through drilling on the surface or shallow underground, and utilizing natural pressure to push the oil and gas resources to the surface[1]. With the continuous depletion of shallow oil resources, the development of deep oil and gas resources has become a research priority. Deep wells are usually less than 2,000 m deep, while ultra-deep wells can be more than 4,000 m deep or even up to 10,000 m deep[2]. To explore for these deep oil and gas resources, explorers must drill deep and ultra-deep wells and use coring operations to obtain more accurate formation information to evaluate oil and gas reserves. Therefore, coring is an important means to provide high-quality data for oil and gas development, and it is of great significance in the exploration and development process[3].

Conventional coring tools can no longer meet the requirements of coring under complex formation conditions, because of the existing conventional coring tools, the design and development of high-strength GQX-type small borehole coring tools. However, during the coring process, the outer tube of the coring tool is easy to be thinned under the erosion of drilling fluid, and then deformed and failed under the axial pressure. Due to the presence of solid particles such as rock chips in the drilling fluid, drilling equipment and downhole tools are highly susceptible to erosion and failure when there is a sudden change in pressure and velocity.

Aiming at the erosion problem in the drilling process, a large number of scholars have carried out simulation and experimental research on erosion[4]. The drilling process can result in damage to drilling equipment because of the working environment, such as erosion, chemical corrosion, friction, radiation corrosion and abrasive wear[5]. Among them, erosion, which is mainly caused by the impact of particles in the drilling fluid, will directly lead to the damage of the material surface, and is the most common mode of failure. The internal structure of drilling tools contains many gaps or cross-sectional mutations that are susceptible to erosion. Structures such as throttle valves[6,7], rotors and stators of mud pulse generators[8,9], hydraulic oscillators[10,11], and drill bits[12,13] have all been studied by scholars. In gas drilling, structures such as columns[14,15], screens[16] and shaped pipes[17,18] are also subject to severe erosion under the influence of

rock cuttings. Many scholars have also conducted erosion experiments, compared the experimental results with simulations, and optimized the erosion models[19-23].

The GQX coring tool is small in size, and the drilling fluid flow path between the inner and outer tubes of the coring is not sufficiently reserved, so when the drilling fluid flow rate is large, it is easy to form a large pressure difference inside the tool. The shunt design of the diverter shaft can smoothly reduce the pressure before the drilling fluid enters the flow path between the outer and inner barrels. The change of drilling fluid flow direction and overflow area at the diverter hole causes the drilling fluid to impact the diverter shaft and outer tube, resulting in erosion. To address this problem, the flow channel model of the diverter shaft part is extracted for numerical simulation to study the influence of different environmental parameters on the erosion rate and optimize the diverter hole structure parameters.

II. MATHEMATICAL MODEL

During coring, the drilling fluid circulates through the drill string and carries cuttings to the surface via the annulus. The flow of drilling fluid could be treated as a two-phase flow of liquid and solids. This work used the Euler-Lagrange method to simulate the liquid-solid flow. The volume fraction of cuttings in the liquid-solid flow at the bottom of the well was less than 10%. Therefore, the Discrete Phase Model was used to simulate the trajectory of the cuttings. When tracking particle trajectory and calculating erosion rate, the following assumptions were made:(1) Fluid is incompressibility; (2) Temperature changes are not considered; (3) Particle breakage is ignored; (4) Collisions between particles are ignored.

Liquid phase model

The continuity equation and the momentum equation are given as:

$$\frac{\partial \rho}{\partial t}+\nabla\cdot\left(\rho\vec{u}\right)=0 \tag{1}$$

$$\frac{\partial}{\partial t}\left(\rho\vec{u}\right)+\nabla\cdot\left(\rho\vec{u}\vec{u}\right)=-\nabla P+\nabla\cdot\left(\vec{\tau}\right)+\rho\vec{g}+\vec{S}_M \tag{2}$$

where ρ is liquid density, $\vec{u}$ is the instantaneous velocity vector, P is pressure, $\vec{\tau}$ is the stress tensor, $\rho\vec{g}$ is the gravitational body force, $\vec{S}_M$ is the added momentum due to the solid phase.

The Realizable k-ε model is one of the standard turbulence models that can more accurately describe turbulent flow near the wall. It has adaptive model parameters, a wide range of applications, and can achieve a balance between computational time and accuracy. The equations of Realizable k-ε model are given as:

$$\frac{\partial\left(\rho k\right)}{\partial t}+\frac{\partial\left(\rho k u_i\right)}{\partial x_i}=\frac{\partial}{\partial x_j}\left[\left(\mu+\frac{\mu_t}{\sigma_k}\right)\frac{\partial k}{\partial x_j}\right]+G_k+G_b-\rho\varepsilon-Y_M+S_k \tag{3}$$

$$\frac{\partial\left(\rho\varepsilon\right)}{\partial t}+\frac{\partial\left(\rho\varepsilon u_i\right)}{\partial x_i}=\frac{\partial}{\partial x_j}\left[\left(\mu+\frac{\mu_t}{\sigma_\varepsilon}\right)\frac{\partial\varepsilon}{\partial x_j}\right]+\rho C_1 S_\varepsilon-\rho C_2\frac{\varepsilon^2}{k+\sqrt{v\varepsilon}}+C_{1\varepsilon}\frac{\varepsilon}{k}C_{3\varepsilon}G_b+S_\varepsilon \tag{4}$$

where G_k is the generation of turbulent kinetic energy due to the average velocity gradient, G_b is the generation of turbulent kinetic energy due to buoyancy, Y_M is the effect of the compressible turbulent pulsation expansion on the total dissipation, u_i is the velocity component in i direction, x_i and x_j are the spatial coordinates, σ_k and σ_ε are the turbulent Prandtl numbers for k and ε, $C_{1\varepsilon}$, C_2 and $C_{3\varepsilon}$ are constants, S_k and S_ε are source terms, μ_t is the turbulent viscosity coefficient, $\mu_t=\rho C_\mu\frac{k^2}{\varepsilon}$ .Here, $C_{1\varepsilon}$ =1.44, C_2 =1.92, $C_{3\varepsilon}$ =0.09, σ_k =1, σ_ε =1.3, $C_1=\max\left[0.43,\frac{\eta}{\eta+5}\right]$, where $\eta=S\frac{k}{\varepsilon}$, $S=\sqrt{2S_{ij}S_{ij}}$.

Discrete-phase model

In FLUENT software, the particle force differential equations in the Lagrangian coordinate system are integrated to obtain the trajectories of solid particles. According to Newton's second law, the governing equations of motion for a unit mass particle are given as:

$$\frac{d\vec{u}_p}{dt}=\vec{F}_D+\vec{F}_B+\vec{F}_P+\vec{F}_{VM} \tag{5}$$

where u_P is the particle velocity, F_D is the flickering force, F_B is the buoyancy, F_P is the pressure gradient force, F_{VM} is the attached mass force.

Particle-wall collision rebound model

According to the erosion model, it is assumed that the energy loss of solid particles only comes from the process of hitting the wall and bouncing back so that the particle's bouncing velocity is less than the velocity before the impact, so it is necessary to use an appropriate model to simulate the energy loss of solid particles. Typically, the tangential and normal coefficients of recovery are used to describe this behavior, which are given as:

$$e_n = \frac{u_{p2}}{u_{p1}} \tag{6}$$

$$e_t = \frac{v_{p2}}{v_{p1}} \tag{7}$$

where u_{p1} is normal velocity components of the particle before impact, u_{p2} is normal velocity components of the particle after impact, v_{p1} is the tangential velocity components of the particle before impact, v_{p2} is the tangential velocity components of the particle after impact.

In this paper, we use the stochastic particle-wall collision rebound model proposed by and Grant and Tabakoff, which is given by:

$$e_n = 0.993 - 1.76a + 1.56a^2 - 0.49a^3 \tag{8}$$

$$e_t = 0.998 - 1.66a + 2.11a^2 - 0.67a^3 \tag{9}$$

Where a is the particle impact angle.

Erosion model

The rate of erosive wear in the inner lumen of the diverter shaft is mainly related to the number of particles, velocity, diameter, mass flow rate, impact angle and collision contact area. The erosion modelling equation is given by:

$$R_{erosion} = \sum_{p=1}^{N} \frac{m_p C(d_p) f(\alpha) v^{b(v)}}{A} \tag{10}$$

where m_p is particle mass flow rate, $C(d_p)$ is particle size function, $f(\alpha)$ is particle impact angle function.

Numerical model

Figure 1 shows a two-dimensional sectional view of the diverter hole portion of the GQX172 coring tool. Wherein the half-ring, bearing, and diverter shaft form a rotating suspension assembly. The bearing is in the upper part of the diverter shaft at the shoulder of the table and is restricted between the bearing bush and the adaptor by the half-ring, which mainly serves to avoid that the inner tube does not rotate with the outer tube. The lower part of the mandrel is equipped with a plugging detection device. Mainly by the flow blocking tube, spring, slipcase and blocking ball valve composition, its role is: when the cardiac jam, the outer tube downward movement and the inner tube in the core of the role of the top, so that the flow blocking tube upward movement blocking the diverter hole and thus generate a pressure difference, according to the pressure difference can be judged to take the heart of the cardiac jam.

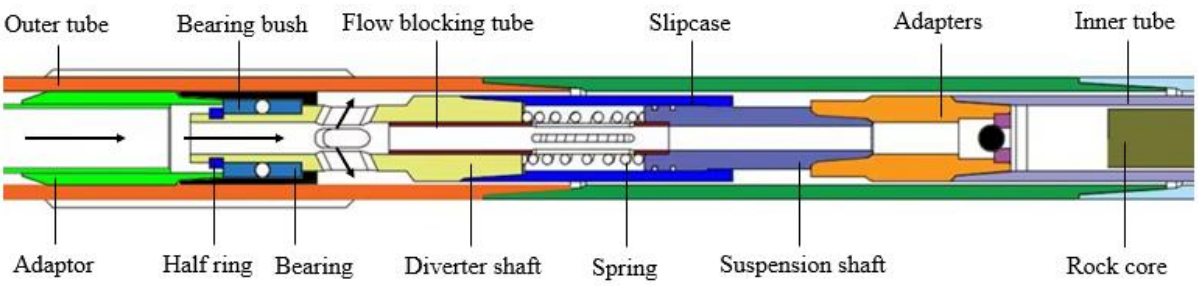

Figure 1 Two-dimensional cross-sectional view of the mandrel section of the coring tool

The drilling fluid flow channel was modeled and meshed as shown in Figure 2. Due to the complex structure at the diverter holes, a polyhedral mesh is selected with a maximum grid cell size of 3 mm and a minimum size of 0.5 mm, and the final mesh number is 374×104.

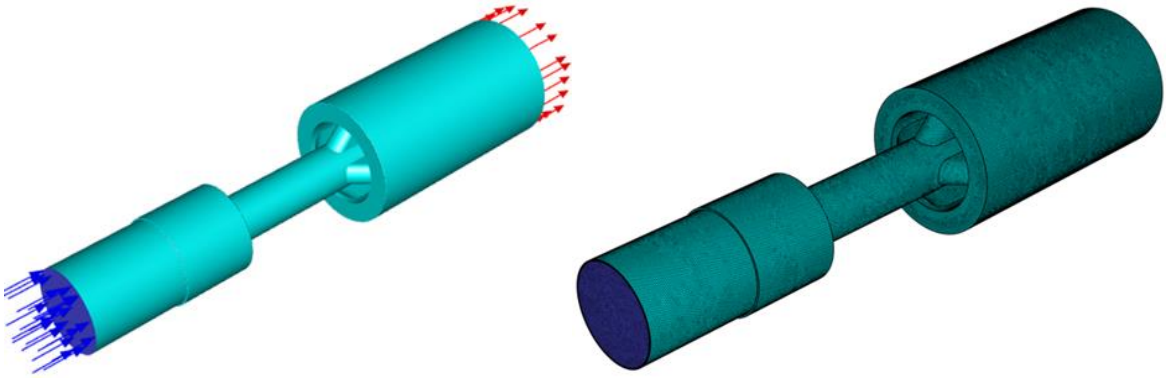

Figure 2 Flow channel 3D model and grid Model

The force-velocity coupling is performed using the Coupled algorithm. Momentum, turbulent kinetic energy, and dissipation rate are solved using Second Order Upwind format. The flow field near the wall is solved using Enhanced wall treatment. The convergence criterion is residuals less than 10^{-4}.

The inlet boundary is set to be velocity inlet, the outlet boundary is set to be free flow, and the wall boundary is set to be no-slip wall. The liquid phase density is 1500 kg/m^3 and viscosity is 0.1 Pa·s. The particle density is 2500 kg/m^3, the discrete phase inlet velocity is the same as the liquid phase velocity, and the type of the discrete phase particles on the wall is set to be reflect.

III. ANALYSIS OF EROSION INFIUENCING FACTOR

Flow field characterization of diverter shaft

The pressure and velocity clouds on the middle section of the diverter shaft for a drilling fluid flow rate of 22 L/s, a particle diameter of 0.6 mm, and a mass flow rate of 0.6 kg/s are shown in Figure 3. At the inlet, the pressure decreases rapidly and the velocity surges due to the reduced overflow area. Along the central flow path to the diverter hole inlet, the pressure and velocity of the drilling fluid change smoothly in this section. At this point, the lower part is blocked, making it impossible for drilling fluid to pass through and creating a high pressure in the central flow path area. The drilling fluid with a high flow rate can only pass through the diverter hole, forming an impact on the inner wall surface of the outer barrel and thus creating erosion.

When the drilling fluid passes through the diverter hole, a large velocity change occurs, and there is a clear zoning of the velocity change above and below the diverter hole, with the velocity change at the top of the hole being small and the velocity change at the bottom being more dramatic. Due to the sudden change of flow direction, the drilling fluid pressure decreases suddenly at the lower wall of the diverter hole, and then gradually stabilizes after flowing through the diverter hole. At the wall opposite to the outlet of the diverter hole, the drilling fluid impacts the inner wall of the outer barrel and the velocity decreases, causing a small increase in pressure near the wall at the impact. The drilling fluid pressure changes smoothly through the central flow path through the diverter shaft to the lower step surface of the diverter shaft, while the velocity changes abruptly at both the overflow area and the change in flow direction.

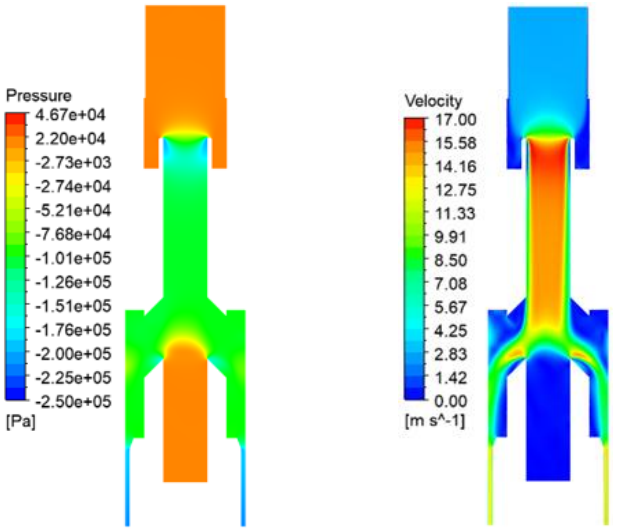

(a) Pressure cloud (b) Velocity cloud diagram

Figure 3 Pressure and velocity clouds for diverter shaft profiles

Figure 4 shows the velocity vector diagram and local enlargement on the middle section of the diverter shaft. When the high-speed drilling fluid enters the diverter hole from the central flow path, the excessive velocity causes a gap between it and the bottom wall of the diverter hole. And a very small vortex is formed at the bottom of the diverter hole as can be seen in the enlarged picture. At the same time, after the drilling fluid passes through the diverter hole and impacts the inner wall surface of the outer barrel, part of the drilling fluid returns upward and forms a vortex at the top of the diverter hole.

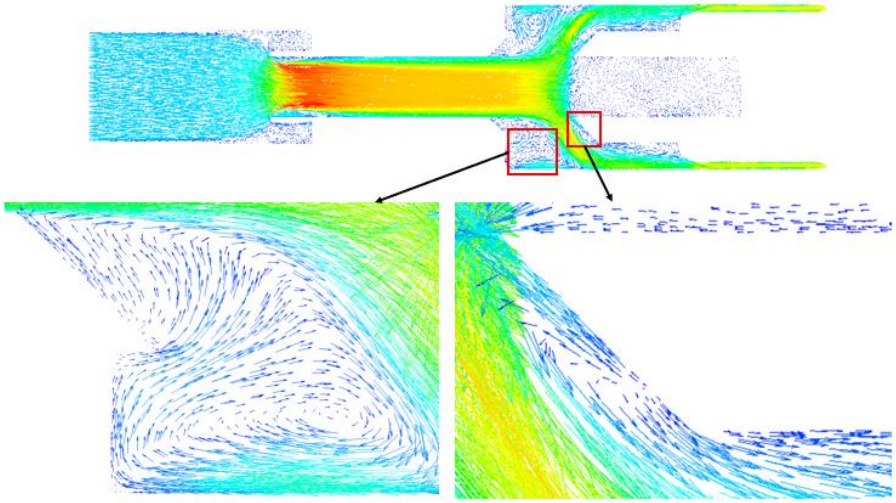

Figure 4 Velocity vector diagram on the middle section of the diverter shaft

Effect of drilling fluid flow on erosion

According to the actual working conditions, the drilling fluid flow rate is 18~25 L/s, and the maximum erosion rate and average erosion rate under different flow rates are shown in Figure 5. The erosion rate and the drilling fluid flow rate is an approximately linear increase in the relationship, this phenomenon is mainly due to the solid particles in the liquid phase of the inertia force with the size of the drilling fluid flow rate. When the flow rate of drilling fluid is slow, the inertia force of the particles is small, so the collision impact on the wall will be relatively small, resulting in a relatively low erosion rate. However, when the flow rate of the drilling fluid is gradually increased, the inertial force on the solid particles in all directions is also gradually increased. This results in an effective increase in the impact strength of the particles on the wall, leading to an approximately linear increase in the final erosion rate.

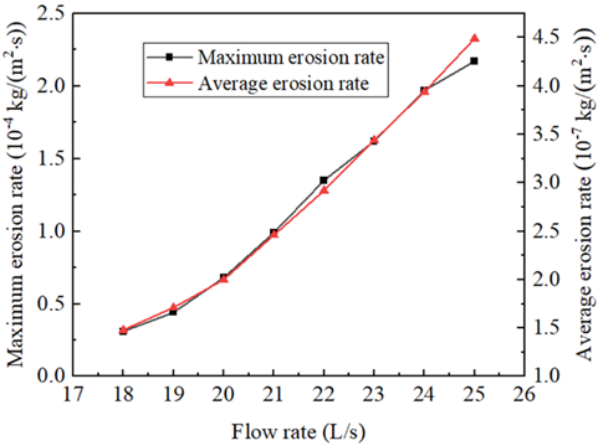

Figure 5 Maximum erosion rate and average erosion rate at different flow rates

Effect of particle size on erosion

The maximum and average erosion rates for different particle diameters are shown in Figure 6. With the increase of particle diameter, the maximum erosion rate gradually increased trend is also gradually enhanced. This is because when the particle diameter becomes larger, the intensity of the collision between the particle and the wall will be strengthened, which will significantly increase the maximum erosion rate. However, the mass flow rate of the particles is a fixed value, the total number of particles is decreasing, so the trend of the average erosion rate is decreasing. When the particle diameter increases to a certain level, both the maximum erosion rate and the average erosion rate will decrease. In the trend of change, the size of the particle diameter is still the main reason for the erosion rate, and its effect on the erosion rate is a dynamic process.

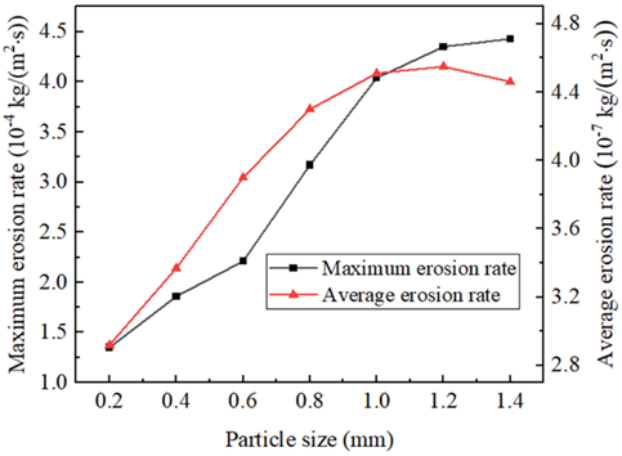

Figure 6 Maximum erosion rate and average erosion rate at different particle sizes

Effect of particle mass flow rate on erosion

The maximum erosion rate and average erosion rate for different particle diameters are shown in Figure 7. There is a clear positive correlation between the maximum and average erosion rates and the particle mass flow rate. This is because as the particle mass flow rate continues to increase, the number of particles per unit volume also increases. This increase leads to a higher probability of particle-wall collision per unit area and thus a higher maximum erosion rate.

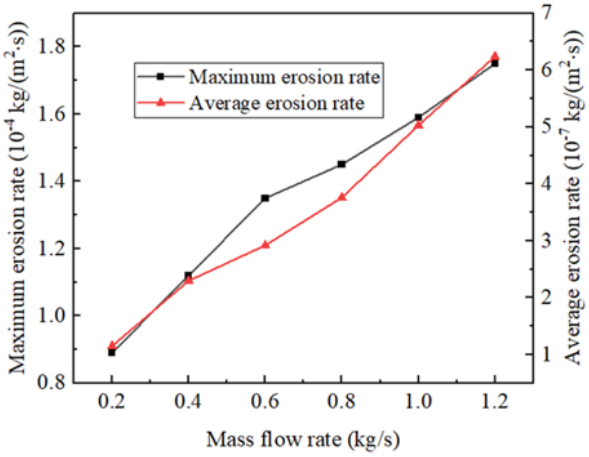

Figure 7 Maximum erosion rate and average erosion rate at different mass flow rates

IV. OPTIMIZATION OF DIVERTER SHAFT STRUCTURE

The structure of the diverter shaft runner is shown in Figure 8, and the main parameters are diverter hole inclination angle θ, length L and width D.

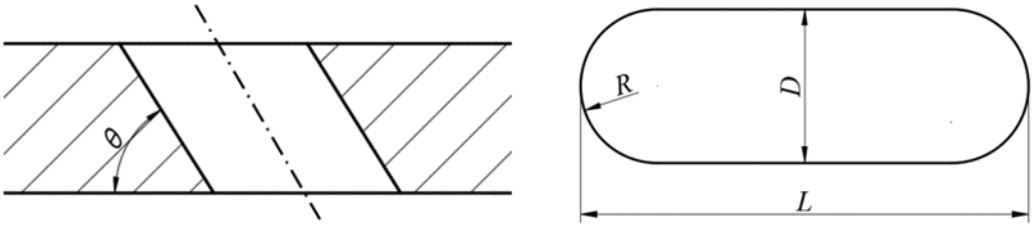

Figure 8 Diverter hole structure

When the inclination angle of the diverter hole is 45°, the length is 70 mm, and the width is 24 mm, the distribution of erosion on the inner wall of the outer barrel is shown in Figure 9(a). When the drilling fluid with high flow rate flows out of the diverter hole, due to the downward tilt of the diverter hole, the drilling fluid drives the solid particles to wash the inner wall of the outer tube, forming a diffuse erosion area. As the outer tube is cylindrical, the impact area of the drilling fluid is a circular curved surface, and the erosion area forms a crescent-shaped curved feature. Erosion was also observed on the inner wall of the outer tube corresponding to the step surface below the diverter shaft, due to the sudden reduction of the overflow area, which caused a sudden increase in the fluid flow rate and erosion on the wall.

The distribution of erosion in the diverter holes is shown in Figure 9(b), in which the erosion area is mainly concentrated in the lower part of the side wall surface of the diverter holes as well as in the wall surface of the connection between the central flow channel and the diverter holes. Combined with the pressure and velocity cloud and velocity vector diagrams, the more obvious erosion area is the same as the location where the sudden change of pressure and velocity occurs. In contrast, the existence of vortices at the upper and bottom of the diverter hole and the small drilling fluid flow rate make the walls at these two locations less eroded.

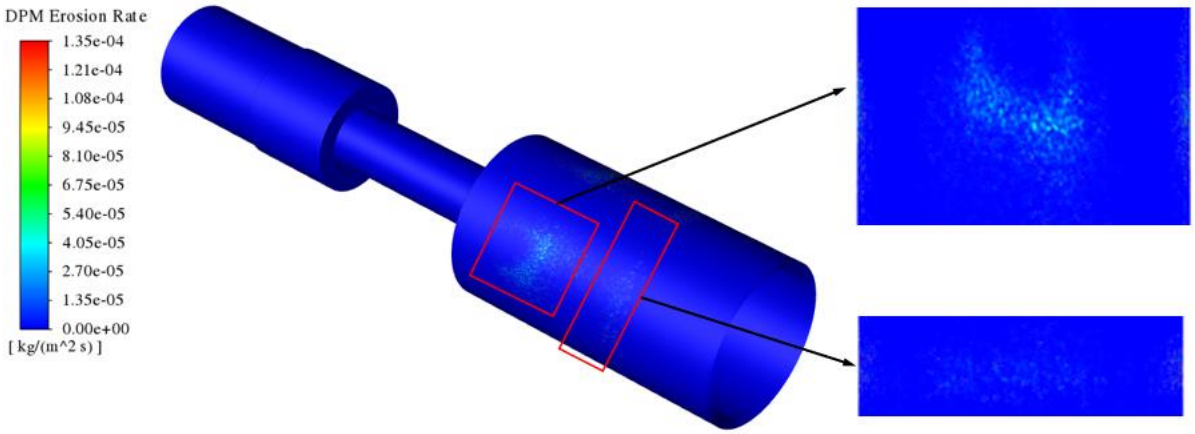

(a)Inner wall of the outer tube

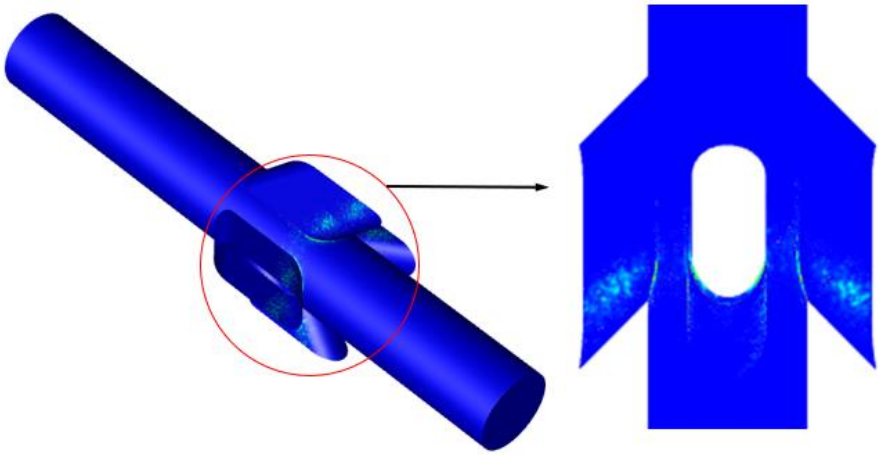

(b) Inner wall of the diverter hole

Figure 9 Cloud map of erosion

Effect of diverter hole inclination angle on erosion

The erosion morphology of the inner wall surface of the outer barrel and the wall surface of the diverter hole when the inclination angle is 15°, 30°, 45°, 60° and 75° are shown in Figure 10 and 11, respectively. From the results of numerical simulation, it can be found that when the inclination angle is 15°, the drilling fluid flows to the outer barrel with a small inclination angle, and the first to be impacted is the upper wall surface of the diverter hole. Compared with the erosion patterns at other angles, the inner wall of the outer barrel is less affected at this time. The wall surface of the diverter hole is more significantly affected by erosion. As the tilt angle increases, the erosion area at the inner wall appears to move downward and the downward spreading tendency is weakened, and a crescent-shaped feature also appears. This feature becomes more and more obvious with the increase of tilt angle. When the tilt angle is 75°, it can be observed that the bottom wall of the diverter hole also shows obvious erosion phenomenon. The size of the tilt angle of the drill bit has a significant effect on the movement path and impact position of solid particles in the drilling fluid.

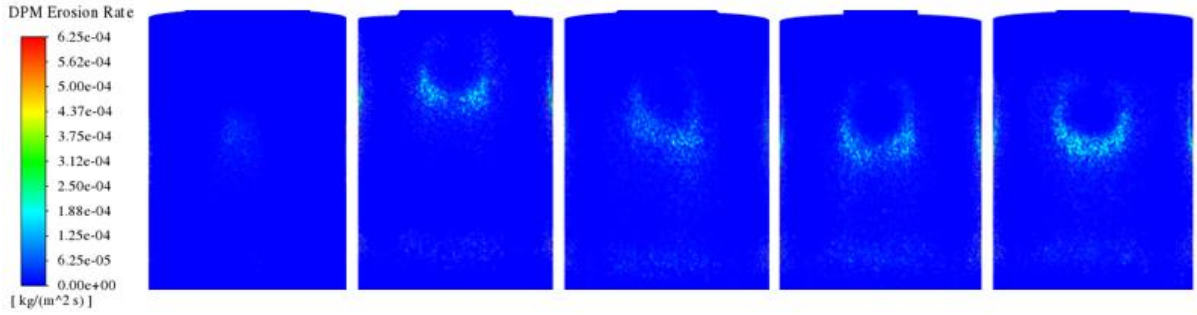

(a)15° (b)30° (c)45° (d)60° (e)75°

Figure 10 The erosion morphology of the inner wall surface of the outer tube at different inclination angles

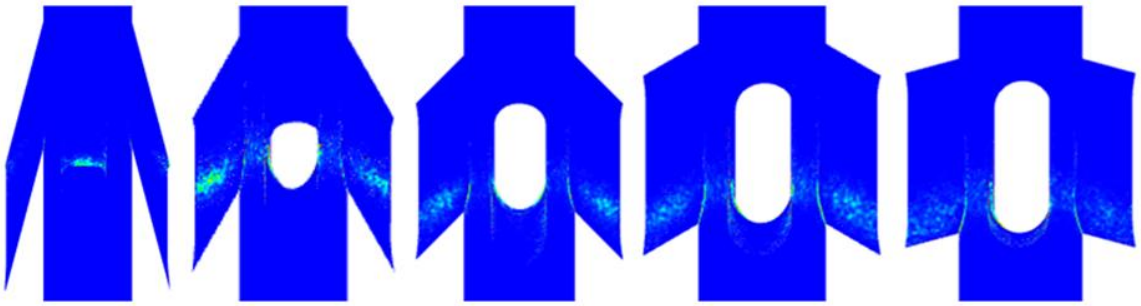

(a)15° (b)30° (c)45° (d)60° (e)75°

Figure 11 The erosion morphology of the inner wall surface of the diverter hole at different inclination angles

The maximum erosion rate and average erosion rate at different angles are shown in Figure 12. The maximum erosion rate shows a rapid decrease and tends to level off with the increase of inclination angle. This is since the drilling fluid enters the diverter hole, the velocity increases, and at a small inclination angle, the drilling fluid will impact on the diverter hole first. Compared with the first impact on the inner wall surface of the outer tube, the drilling fluid has a greater velocity at this time, resulting in the phenomenon of a large maximum erosion rate. As the angle of inclination increases, the pressure and velocity changes of the drilling fluid passing through the diverter hole gradually stabilize, so the maximum erosion rate decreases and tends to level off.

The average erosion rate, on the other hand, decreases and then increases, and there is a minimum value in the range of inclination angle of 40°~50°. From the erosion topography of the manifold, the direction of velocity change is basically constant when the drilling fluid passes through the manifold. When the inclination angle is small, there are large vortices above and below the manifold, and the undulation of the drilling fluid flow becomes larger, so that the wall of the manifold is subjected to larger erosion. When the tilt angle is larger, the drilling fluid passes through the bottom of the diverter hole, and the inner wall of the outer tube is more eroded. Overall, when the tilt angle and drilling fluid velocity direction is close to, so that the erosion of these two places are more balanced, there is a phenomenon that the average erosion rate first decreases and then increases.

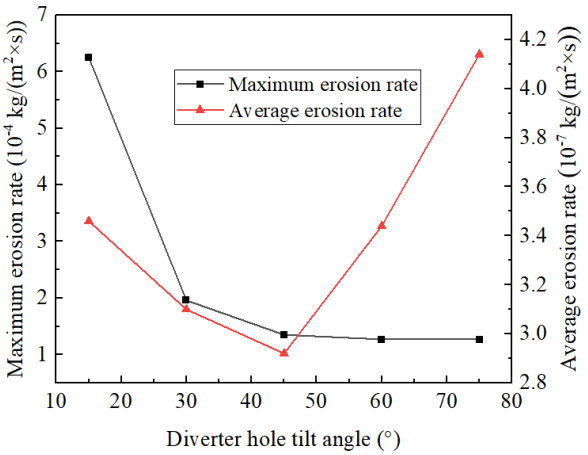

Figure 12 Maximum erosion rate and average erosion rate at different angles

Effect of diverter hole width on erosion

The erosion morphology of the inner wall surface of the outer tube with different diverter hole widths is shown in Figure 13. With the increase of the width, the width of the erosion area does not show obvious changes, and the shape of the erosion changes from crescent-shaped to dumbbell-shaped, with obvious differences between the two sides and the center. This is because the two sides of the exit area of the diverter hole are low-pressure areas, and the drilling fluid will spread to the two sides of the diverter hole after flowing out of the diverter hole to appear the separation phenomenon. As the width increases, the tendency of this separation accelerates. When the width is small, the drilling fluid is impacted on the wall before separation, and the erosion area is more continuous currently. When the width is large, the drilling fluid is separated before it collides with the wall, and a dumbbell-shaped erosion area appears. Therefore, the increase in the width of the diverter hole will also affect the erosion morphology of the outer tube.

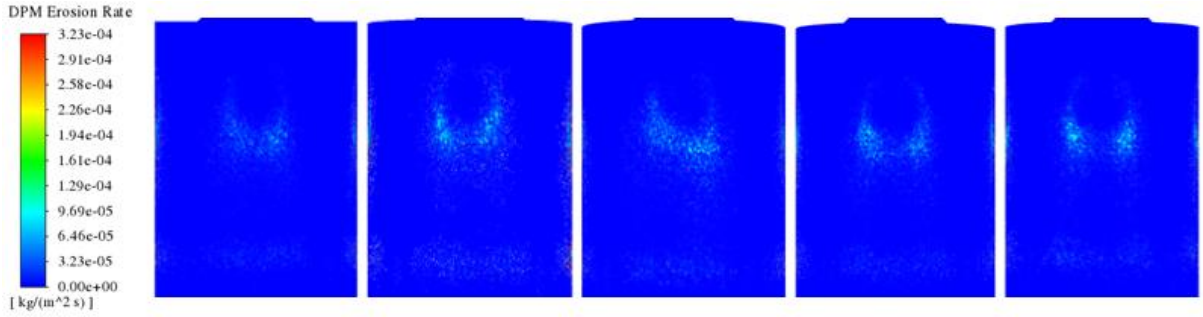

(a) 20mm (b) 22mm (c) 24mm (d) 26mm (e) 28mm

Figure 13 The erosion morphology of the inner wall surface of the outer tube with different diverter hole widths

The maximum erosion rate and average erosion rate at different manifold widths are shown in Figure 14. The velocity and flow rate of drilling fluid through the diverter hole will change with the change of diverter hole width. With a smaller width, the flow rate of drilling fluid is larger, which causes more intense erosion of its wall. Therefore, a smaller hole width results in a higher erosion rate. As the hole width increases, the throttling effect decreases and the velocity of the drilling fluid decreases. Although the drilling fluid flow rate through the diverter hole increases, the overall fluid impact area also expands, so the erosion rate is decreasing. When the width of the diverter hole is increased to a certain degree, the throttling effect basically disappears, and the drilling fluid flow rate through the diverter hole reaches the maximum value. At this time, the flow rate is low and will not produce more violent erosion on the wall, and the erosion rate will tend to be smooth. In addition, the increase in the width of the diverter hole may also lead to the formation of more complex vortices in the region between the diverter shaft and the outer tube. This makes the calculation process difficult to converge and influences the erosion on the inner wall surface. Therefore, rational design and optimization is required to select the appropriate size of the diverter hole to achieve the best throttling effect and reduce the erosion losses.

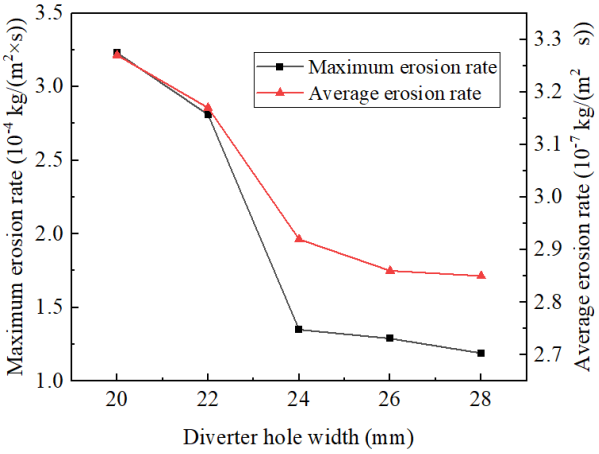

Figure 14 Maximum erosion rate and average erosion rate at different diverter hole widths

Effect of diverter hole length on erosion

The erosion morphology of the inner wall surface of the outer tube for different diverter hole lengths is shown in Figure 15. As the length of the diverter hole increases, the upper low velocity zone will become wider due to the inertia of the fluid flow, which will result in the formation of vortices with a consequent widening of the radius. At the same time, the diverter hole will disturb the flow of drilling fluid and make the flow more unstable. This unstable flow will also cause erosion of the drilling fluid on the inner wall of the outer tube. As the bottom surface of the manifold moves downward, the erosion area also moves downward and becomes longer, and spreads to both sides.

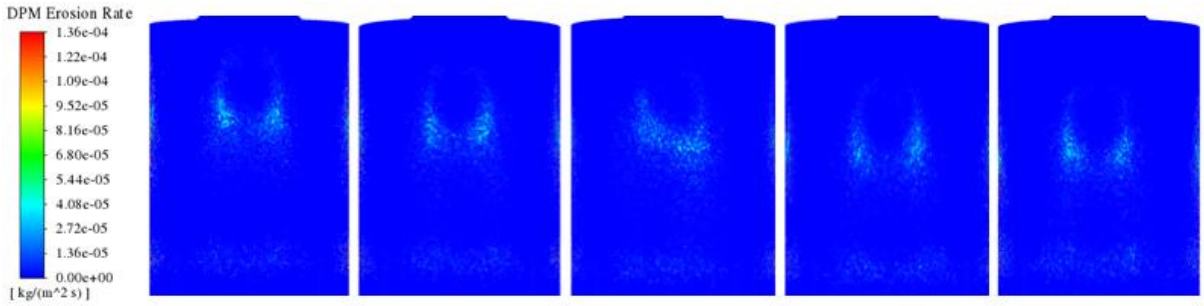

(a)60mm (b)65mm (c)70mm (d)75mm (e) 80mm

Figure 15 The erosion morphology of the inner wall surface of the outer tube with different diverter hole lengths

The maximum erosion rate and average erosion rate at different diverter hole lengths are shown in Figure 16. It can be seen that the average erosion rate is distributed in the range of 2.9×10^{-7}~3.0×10^{-7} kg/(m^2 ·s), and the maximum erosion rate is distributed in the range of 1.2×10^{-4} ~1.4×10^{-4} kg/(m^2 ·s). Although both erosion rates decreased with the increase of the length of the diverter hole, the overall change was not significant.

Compared with other structural parameters, the influence of the length of the manifold is small, and the erosion rate tends to stabilize when it is larger than 65 mm. In the process of design and application, if the length of the diverter hole meets the strength requirements, it can meet the requirements of the erosion rate control.

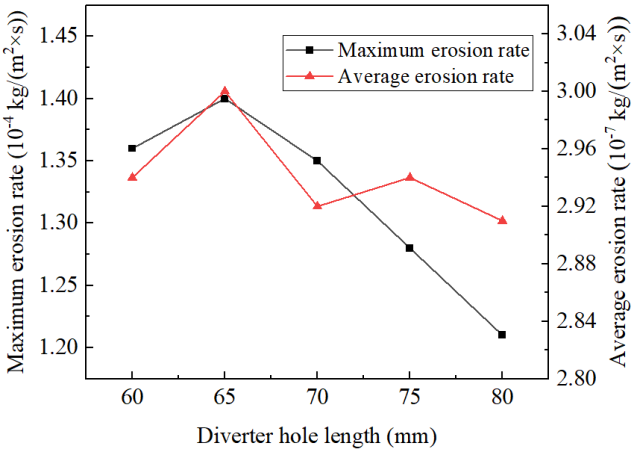

Figure 16 Maximum erosion rate and average erosion rate at different diverter hole lengths

Effect of number of diverter holes on erosion

The erosion morphology of the inner wall surface of the outer cylinder and the wall surface of the diverter hole for different numbers of diverter holes is shown in Figures 17 and 18. With the increase of the number of holes, the erosion region on the wall surface of the outer cylinder is obviously reduced, and the shape changes from the initial mass to crescent shape, and finally presents a dumbbell shape. This indicates that the shape of the erosion region gradually becomes more regular and concentrated with the increase of the number of holes. When the number of holes is 2, the erosion region on the wall surface of the diverter holes covers most of the wall surface of the diverter holes and the wall surface of the center runner between two diverter holes. Increasing the number of holes, causes the erosion region to shrink towards the lower part of the diverter holes, When the number of holes is 6, only the connection between the diverter holes and the center runner wall receives the most significant erosion compared to other regions.

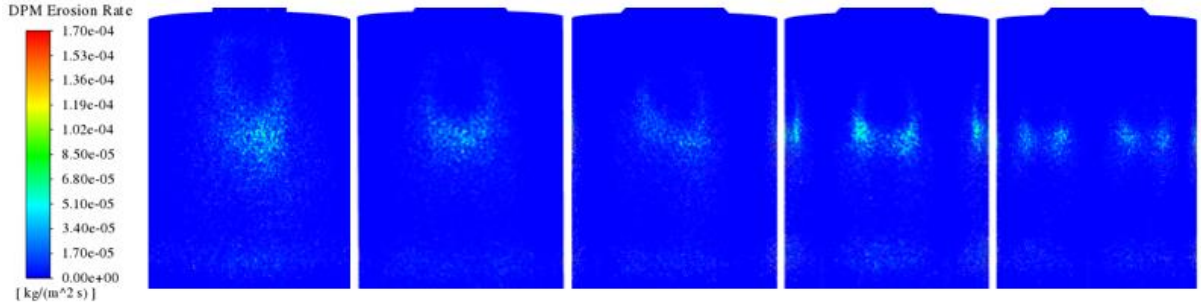

(a)2 (b)3 (c)4 (d)5 (e)6

Figure 17 The erosion morphology of the inner wall surface of the outer tube at different diverter hole numbers

(a)2 (b)3 (c)4 (d)5 (e)6

Figure 18 The erosion morphology of the inner wall surface of the diversion hole at different diverter hole numbers

The maximum and average erosion rates for different numbers of diverter holes are shown in Figure 19. The average erosion rate decreases significantly as the number of holes increases, while the maximum erosion rate fluctuates. In the number of holes for 3 when there is a small value, and then increase again after it has been reduced. From the change rule of erosion rate can be seen, the number of holes should be increased appropriately. When the number of diverter holes is small, the flow rate of drilling fluid through the diverter holes will be relatively large, which will produce very strong and large erosion on the wall. There will also be a large energy loss and a large differential pressure. On the contrary, when the number of diverter holes is increased, the velocity of the fluid passing through a single diverter hole will be reduced, the energy loss will be relatively small, and the pressure consumption will be small. If the pressure difference between the inlet and outlet is the same, increasing the number of diverter holes can increase the flow rate of drilling fluid, which helps to improve the efficiency of drilling work. However, increasing the number of diverter holes will reduce the strength, so the number of diverter holes should be increased as much as possible while considering the structural safety.

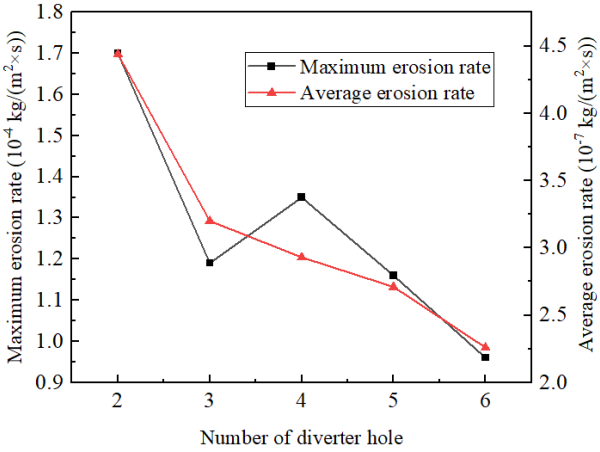

Figure 19 Maximum erosion rate and average erosion rate at different diverter hole numbers

V. CONCLUSION

(1) Maximum erosion rate and average erosion rate, grow approximately linearly with both flow rate and mass flow rate. The maximum erosion rate increases faster with different drilling fluid flow rates, and the average erosion rate increases faster with different mass flow rates. When the diameter of the particles changes, the growth trend of the average erosion rate is slowing down and the maximum erosion rate is speeding up. Since the mass flow rate is constant, both decrease when the diameter increases to a certain extent.

(2) The parts of the diverter shaft that are susceptible to erosion are the lower part of the side wall of the diverter hole and the wall at the connection between the diverter hole and the center runner, while the parts of the inner wall of the outer cylinder that are susceptible to erosion are the areas corresponding to the lower part of the diverter hole along the direction of the diverter hole tilting angle and the lower part of the diverter hole and the erosion areas show crescent-shaped features.

(3) The erosion pattern of diverter holes is investigated at different inclination angles, widths, lengths, and numbers. The tilt angle in the range of 40°~50° can make the erosion rate down to a smaller range. At the same angle, the width and the number of holes have a significant effect on the erosion rate, and the values of both should be as large as the strength allows. And although the length has less effect on the erosion, it is also recommended to be greater than 65 mm.

REFERENCE

[1]. Xie H, Liu T, Gao M, et al. Research on in-situ condition preserved coring and testing systems[J]. Petroleum Science, 2021, 18(6):1840–1859.
[2]. Cardoe J, Nygaard G, Lane C, et al. Oil and gas drill bit technology and drilling application engineering saves 77 drilling days on the world's deepest engineered geothermal systems egs wells[C]. SPE/IADC International Drilling Conference and Exhibition, 2021.
[3]. Guo D, Xie H, Gao M, et al. In-situ pressure-preserved coring for deep oil and gas exploration: Design scheme for a coring tool and research on the in-situ pressure-preserving mechanism[J]. Energy, 2024, 286:129519.
[4]. Liu L, Wang Y, Zhang K, et al. Uneven wear behavior of downhole tool clearance material under slurry erosion[J]. Alexandria Engineering Journal, 2023, 73:47-68.
[5]. Surbled A. 10-A monitoring management strategy in tribocorrosion: Application to erosion-corrosion in oil and gas exploration-production[J]. Mechanical and Electro-Chemical Interactions Under Tribocorrosion, 2021, 227-258.
[6]. Hu G, Zhang P, Wang G, et al. Performance study of erosion resistance on throttle valve of managed pressure drilling[J]. Journal of Petroleum Science and Engineering, 2017, 156:29-40.
[7]. Wang G, Chu F, Tao S, et al. Optimization design for throttle valve of managed pressure drilling based on CFD erosion simulation and response surface methodology[J]. Wear, 2015, 338:114-121.
[8]. Zhang W, Tian J, Liu B, et al. Erosive wear characteristics and damage model of polycrystalline diamond compact for enhancing mud

pulser rotor[J]. Geoenergy Science and Engineering, 2023, 227:211873.
[9]. Zhang W, Zhang S, Dai W, et al. Erosion wear characteristics of cemented carbide for mud pulser rotor[J]. International Journal of Refractory Metals & Hard Materials, 2021, 101.
[10]. Li K, Peng J, Li Y, et al. Performance prediction of solid particle erosion in fluidic oscillators for fluidic hammers based on CFD-DPM[J]. Powder Technology, 2023, 428:118819.
[11]. He J, Zhang P, Yin Q, et al. Study of drilling muds on the anti-erosion property of a fluidic amplifier in directional drilling[J]. Frattura ed Integrita Strutturale, 2015, 34:564-573.
[12]. Liu W, Bell A, Wang Z, et al. Evaluation of the slurry erosion resistance of the body materials of oil & gas drill bits with a modified abrasive waterjet[J]. Wear, 2020, 456:203364.
[13]. Mao L, Cai M, Liu Q, et al. Effects of spherical WC powders on the erosion behavior of WC-Ni hardfacing used for steel body drill bit[J]. Surface & Coatings Technology, 2021, 409:126893.
[14]. Yan W, Li F, Leng G, et al. Sand control screen erosion-failure prediction method in weakly consolidated sandstone reservoir[J]. Geoenergy Science and Engineering, 2023, 224:211616.
[15]. Amadi A, Mohyaldinn M, Ridha S. Sand particle induced erosion in oil and gas screens: A review of influencing factors and wear dynamics[J]. Powder Technology, 2024, 436:119528.
[16]. Liu H, Liu P, Fan D, et al. A new erosion experiment and numerical simulation of wellhead device in nitrogen drilling[J]. Journal of Natural Gas Science and Engineering, 2016, 28:389396.
[17]. Khan R, Petru J, Seikh A. Erosion prediction due to micron-sized particles in the multiphase flow of T and Y pipes of oil and gas fields[J]. International Journal of Pressure Vessels and Piping, 2023, 206:105041.
[18]. Mao L, Cai M, Wang G, et al. Effect of rotation speed on the abrasive–erosive–corrosive wear of steel pipes against steel casings used in drilling for petroleum[J]. Wear, 2018, 410:1-10.
[19]. Wei N, Meng Y, Li G, et al. Cuttings-Carried theory and erosion rule in gas drilling horizontal well[J]. Thermal Science, 2014, 18:1695-1698.
[20]. Huang Z, Xie D, Huang X, et al. Analytical and experimental research on erosion wear law of drill pipe in gas drilling[J]. Engineering Failure Analysis, 2017, 79:615-624.
[21]. Yang S, Fan J, Liu M, et al. Research on the solid particle erosion wear of pipe steel for hydraulic fracturing based on experiments and numerical simulations[J]. Petroleum Science, 2024.
[22]. Mazen M, Faris S, Farzin D, et al. Experimental and Numerical Studies on the Influence of Particle Sizes on Erosion of Elbows in Series in Gas-Solid and Multiphase Flow Conditions[C]. AMPP Annual Conference + Expo, Denver, Colorado, USA, March 2023.
[23]. Zhao J, Zhang G, Xu Y, et al. Experimental and theoretical evaluation of solid particle erosion in an internal flow passage within a drilling bit[J]. Journal of Petroleum Science and Engineering, 2018, 160:582-596.